**Supplementary Information**

# Colloidal Nafion™ particles: Are Cylinders Ubiquitous?

**SANS analysis**

There are several factors used to describe models for fitting scattering data from a dispersion of discrete particles. These are the particle number density per unit volume, $N$ ($cm^{-3}$), the contrast of the particles ($\rho_p$) relative to the dispersion fluid or solvent ($\rho_s$) $\Delta\rho$ ($cm^{-2}$), the average particle volume, $V_p$ ($cm^3$), the form factor for a single particle, P($Q$), and the structure factor, S($Q$) that describes the effects of the particle interactions on the scattering intensity. The product of these factors accounts for the observed scattering as,

$$I(Q) = N\langle V_p^2 \Delta\rho^2 P(Q) S(Q)\rangle \ (cm^{-1}), \qquad (1)$$

where the angle brackets indicate an average over the population of particles, including their orientations. For the scattering length densities, the values of $\rho$ for each component can be computed from the chemical composition and density, as $\rho = \Sigma b_i/V$. The sum is over the number of scattering centers with scattering length $b_i$ (cm), and, $V$, is the particle volume. The form factor P($Q$) is the square of the Fourier transform of the particle structure normalized to $V_P$. The structure is the distribution of scattering length density, $\rho$(r), defined by the particle shape and its density fluctuations. A graphical representation of the individual products in **Eq (1)** is shown in **Figure S1a.**

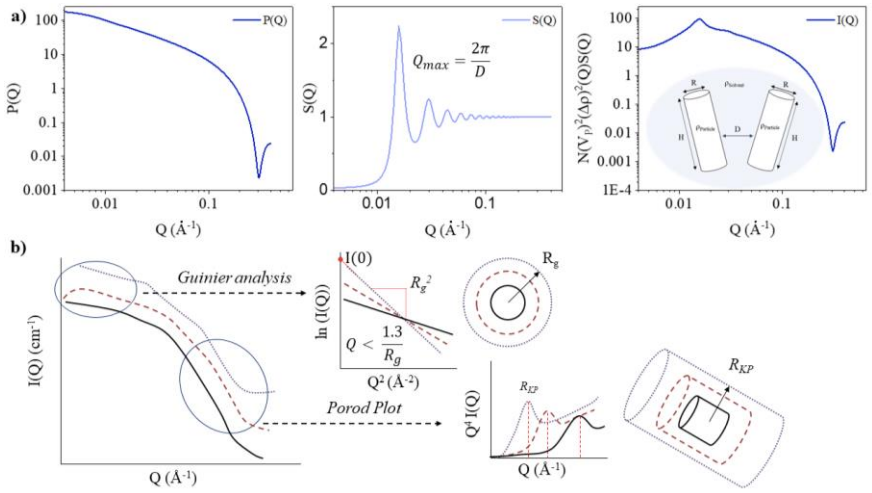


**Figure S1:** Illustration of the scattering analysis. a) cylindrical form factor P($Q$) (left), structure factor S($Q$) (center) and the resulting theoretical scattering profile calculated as per **Eq (1)** (right). b) The low- and high-$Q$ scattering region graphical analysis techniques (Guinier plots and Porod plots), highlight the trends that indicate differences in particle sizes.

The form of **Eq (1)** for scattering data presents a difficult problem, as in general, the calculations for S($Q$) involve approximations that have a limited range of validity.[1] We tackle SANS data analysis using simplifying assumptions. For the low Q range of the SANS data I(q), when the ratio $QR_g < 1.3$ is satisfied, the Guinier approximation can be used to estimate some structural parameters of a particle (assuming monodisperse system)

$$I(Q) = I(0)\exp(-R_g^2Q^2/3) \qquad (2)$$

where I(0) is the value of intensity extrapolated $Q = 0$, which for the solvent of particles can be interpreted as following:,

$$I(0) = NV_p^2\Delta\rho^2 = \Phi V_p\Delta\rho^2 \text{ (cm}^{-1}\text{)}. \qquad (3)$$

Here, $\Phi$ is the particle volume fraction (calculated from the Nafion™ ionomer density and its dispersion wt%). Linearization of **Eq (2)** allows for the graphical analysis of SANS data, a so called Guinier plot (ln(I(0)) vs $Q^2$) is shown in **Figure 1b**.

The parameters calculated from the Guinier analysis allows estimate structural dimensions of a particle in solution assuming it is a rigid cylinder of radius, $R$, and height, $H$ (Å). This model is chosen based on results published previously on study of the dispersions of the $Na^+$ form of Nafion™ in glycerol or 2-propanol.[2-6] For the rigid cylinder, $V_p = \pi R^2H$ and $R_g^2 = R^2/2 + H^2/12$. Application of the Guinier **Eq (2)** to the data gives two values, $R_g^2$ and I(0). The latter is related to the volume fraction, particle volume, and SLD contrast in **Eq (3)**. $R_g^2$ relates two unknowns, $R$ and $H$, through the solution of a cubic equation, **Eq (4)** in $H$, as,

$$H^3 - 12R_g^2H + 6\,I(0)/\kappa = 0, \text{ (Å}^3\text{)} \qquad (4)$$

where, $\kappa = \pi\Phi\Delta\rho^2$, is easily calculated from the ionomer chemistry, density, and dispersion wt%.

**Eq (4)** has two positive roots, only one of which gives values of $H$ and thus $R$—through the measured $R_g$ and $I(0)/\kappa = V_p/\pi$. A solution for **Eq (4)** that gives a consistent solution for $H$, and thus $R$, is an important guide to an appropriate model.

While the Guinier approximation is useful in determining overall particle size, global shape and contrast, additional structural details are not captured in the analysis due to the limited low-Q range over which the analysis applies. Other details, such as the morphology, require other analysis using detailed models. We use the NIST Center for Neutron Research (NCNR) SANS analysis Macros for Igor Pro [7] to perform the form factor fitting procedures and explore the details of plausible structures consistent with the SANS data.

In some cases, the analysis cannot start with the Guinier plot due to the presence of an ionomer peak in the SANS data corresponding to an interparticle correlation distance in the dispersion. We consider two possibilities to model these cases.

The structure factor S($Q$) of equation (1) due to particle interactions is one possible case. Our complete analysis of the dispersion morphology included calculation of S($Q$) with our program, ChgdHardCyl, using the decoupling approximation[8] with either the Perkus-Yevick closure for hard particle interactions, [9,10] or the BPRMSA approximation for charged particles. [11-15]

Complimentary information regarding an assumed cylindrical morphology can be gathered through a $Q^4$ graphical analysis (Porod plot), represented in **Figure S1b**. Oscillations in the Porod plot can indicate a particle radius through

$$Q_{I(Q)max} r = 2.16 \qquad (5)\ [16]$$

a) Hammouda model Fits

We consider a model of an open chain structure proposed by Hammouda et al. [17] given as

$$\frac{d\Sigma(Q)}{d\Omega} = \frac{A}{Q^n} + \frac{C}{1+|Q-Q_0|L^m} + B \qquad (6$$

Here, the first term accounts for a power law due to a large length scale structure. The second term describes local chain structure due to polymer swelling by interactions with the solvent, leading to a network with characteristic length, L, between crosslinks that give rise to the peak at $Q_0$. The exponent $m$ is taken as a measure of the chain conformation between crosslinks. The final term is to account for incoherent background scattering. The Hammouda equation was encoded into Origin Pro and used as a nonlinear fitting equation. The entire Q-range of data was fit during the procedure. A, n, C, L, $Q_0$, and m were varied during the final fitting procedure, while the incoherent background was fixed after an initial parameterization.

b) Form Factor Model Fits

Form factor models for each of the datasets were developed by first determining the volume fraction of Nafion™ in the dispersion from the weight percentage of the original dispersion. The volume fraction was used to fix the scale in the form factor model. Original values for the radius and height of the particle were determined from the Guinier analysis. To start the particle SLD was specified to be the value of Nafion™ at a density of 2.01 g/cm$^3$ (4.033 x $10^{-6}$ Å$^{-2}$). Solvent SLDs were calculated for the solvents at their bulk density; Water (-0.559 x $10^{-6}$ Å$^{-2}$) and NMP (0.922 x $10^{-6}$ Å$^{-2}$). The background scattering was estimated based on the high $Q$ data. The models were

then fit to the experimental data using the Igor Pro Macros developed by NIST by allowing only the particle radius, height, and SLD to vary. Upper and lower limits on the SLD were determined by the SLD of the solvent and Nafion™, respectively.

*Cylindrical form factors:* The scattering from a right circular cylinder with constant SLD is given by Eq. 7, which assumes S(Q) = 1 and pulls the volume and number density terms of Eq 1 into one form factor. Which is supported by the NIST Igor Pro Macros, and refers to[18]

$$P(Q) = \frac{\Phi}{V_{cyl}} \int_0^{\pi/2} \left(2\Delta\rho V_{cyl} j_0(QH\cos\alpha) \frac{J_1(QR\sin\alpha)}{(QR\sin\alpha)}\right)^2 \sin\alpha \, d\alpha \qquad (7)$$

Where Φ represents the volume fraction of the particle, $V_{cyl}$ is the volume of the cylinder, Δρ is the SLD contrast between particle and solvent, $j_0(x) = \sin(x)/x$, is the zero-order spherical Bessel function, H is the cylinder height, α is the cylinder axis angular position relative to vector **Q**, R is the radius, and $J_1$ is the first order Bessel function. For the SANS of Nafion™ in water, the polydispersity of the radius was allowed to vary during fitting between 0 and 1. Incorporating the polydispersity into the form factor is completed with an additional integration over f(R), the normalized Schulz distribution of the radius, to compute the average value of $V_p^2 P(Q)$, as $\int_{R_{min}}^{R_{max}} V_p^2(R) P(R,Q) dR$ . The radius distribution can be calculated using the polydispersity and the normalized Schulz distribution through Eq 8:

$$f(R) = (z+1)^{z+1} X^z \frac{exp[-(z+1)X]}{R_{avg}\Gamma(z+1)} \qquad (8)$$

where z is related to the polydispersity by $z = (1/p^2)-1$, X is $R/R_{avg}$ (where $R_{avg}$ is provided by the form factor model), and $\Gamma(z+1)$ is the Gamma function. Once again, this equation is supported by the NIST small angle scattering Macros and refers to[18].

*c) Scattering from Fuzzy Spheres*:

The theoretical scattering for a fuzzy sphere contains three terms, a sphere, a soft interface with exponential like profile and a Ornstien-Zernili fluctuations term, given by Eq. 9, included in the NIST Igor Pro Macros referring to[19]

$$I(Q) = \frac{\Phi}{V}\Delta\rho^2 \langle \frac{3[\sin QR - QR\cos QR]}{QR^3} exp\left(\frac{-(\sigma_{surf}Q)^2}{2}\right)\rangle^2 + \frac{I_{lor}(0)}{1+\xi^2 Q^2} \qquad (9)$$

Where Φ represents the volume fraction of the particle, V is the volume of the particle, Δρ is the SLD contrast between particle and solvent, R is sphere radius where ρ has decreased to ½ of the core ρ, < > represents an average over the size distribution, $\sigma_{surf}$ represents the fuzziness of the

Commented [RH1]: .The first term should be jo(QH/2*cos(alpha)). The use of the spherical Bessel function here is formally more correct than my use of the unnormalized sinc function. The volume fraction, volume and contrast should not be included in P(Q) as NVp = phi and the remaining Vdeltarho is included in eps 1 & 3. There should be a factor of 16 outside the integral replacing the 2 in the brackets (see eq . A.22 in the enclosed file.

Commented [RH2]: Physically, what do you mean by this? How is this number related to the parameters in the Schulz distribution?

particle interface, and the final Lorentzian term accounts for fluctuations due to the microgel network with ξ being the correlation length.

d) Guinier Analysis

Guinier Analysis was completed by graphing the data as ln(I(Q)) vs. $Q^2$ and isolating only the low Q data where linearity was observed. Using the Origin graphing and analysis software, a line was fit to the data.

## METHODS

### Small angle neutron scattering

SANS measurements of Nafion™ dispersions in NMP and water were carried out on the SANS instrument, Bilby using the instrument time-of-flight (TOF) beam option,[2] at the Australian Center for Neutron Scattering of the Australian Science and Technology Organization. All measurements were done at a single instrument configuration as the instrument features detector banks that cover the entire required domain of scattering angles, $2\theta$, in one measurement Additional SANS data were collected on the TOF low-Q diffractometer (LQD) at the Manuel Lujan Jr. Scattering Center at Los Alamos National Laboratory.[3,4] Samples were placed in 1 mm path-length fused silica cells (Helma). All measurements were carried out at ambient temperature.

Raw scattering intensity data acquired by the measurements on Bilby were reduced to absolute values of differential scattering cross section per unit steradian per unit volume, I($Q$) ($cm^{-1}$) as a function of scattering wave number, $Q = 4\pi/\lambda \sin\theta$ using standard instrument procedures written using a framework of a package called Mantid, [5] with those on LQD reduced using the Los Alamos developed procured, SMR. [3,4]

### Dispersion preparation

Two acid-form ($H^+$) Nafion™ dispersions in NMP were prepared for SANS measurements. First, a dispersion was prepared by completely evaporating the solvent of the ionomer stock (D520) using a vacuum oven at 80 °C. The resulting solids were taken up to 20 wt% in NMP at 80 °C. This procedure resulted in a clear dispersion, then diluted with additional NMP to obtain 2.5 wt%, measured on Bilby and hereon referred to as a stock transfer dispersion. An alternative dispersion was prepared by boiling the $H^+$ form of Nafion™ 212 membrane (purchased from Fuel Cell Stores) in water for 2 hours, drying it in a convection oven at 80 °C, cutting it into smaller pieces, and then mixing it with NMP and allowed to form a clear 2.5 wt% homogenous dispersion, so-called redispersed membrane, measured on LQD.

The acid form of Nafion™ in water was produced from a stock dispersion of, DE-521 ($H^+$ form, Dupont). The stock solution is nominally 5 wt% a 50:50% mixture of water and 1-propanol. The alcohol, including a small amount of ethanol, was removed by extensive dialysis of 10 ml of the stock dispersion against three, 200 mL changes of deionized water over a three-day period. The

result was a clear dispersion, determined to be approximately 2.6 wt% from a measurement of the carefully measured volume recovered from the dialysis tube.

**Molecular Dynamics**

We employed fully atomistic molecular dynamics using the LAMMPS program.[6] In this work, each system contains 5 Nafion™ chains (6903 g mol$^{-1}$ with 6 pendant side chains each of equivalent weight 1150 g mol$^{-1}$ in a box of solvent at ~ 5 wt% of Nafion™. To keep the system neutral, the charges on the sulfonic group were compensated by 30 hydronium molecules in each simulation box. Herein, periodic boundary conditions were imposed in all three directions. We used the Class II force field equation for bonded and non-bonded interactions. The form of force field used in this study is shown below:

$$E = \sum_{bond} [\, K_{b2}\,(b-b_0)^2 + K_{b3}\,(b-b_0)^3 + K_{b4}(b-b_0)^4]$$
$$+ \sum_{angle} [\, K_{a2}\,(\theta-\theta_0)^2 + K_{a3}\,(\theta-\theta_0)^3 + K_{a4}(\theta-\theta_0)^4]$$
$$+ \sum_{torsion} [\, K_{t1}\,(1-\cos(\varphi)) + K_{t2}\,(1-cos2\varphi) + K_{t3}(1-cos3\varphi)]$$
$$+ \sum_{ij}\left\{ \varepsilon_{ij}\left[2(\frac{\sigma_{ij}}{r_{ij}})^9 - 3(\frac{\sigma_{ij}}{r_{ij}})^6\right] + \frac{q_i q_j}{r_{ij}}\right\}$$

where $b$, $\theta$ and $\varphi$ are the internal coordinates of bond, angle and torsion angle, respectively. The $K_b$, $K_a$ and $K_t$ are the force constants for bond, angle, and torsion terms. The last two terms of the equation represent the non-bond interactions, viz., van der Waals (vdW) (LJ-9-6) and Coulombic interactions.

The mixing rules below are applied for cross terms in vdW equation.[7]

$$\sigma_{ij} = \left(\frac{\sigma_i^6 + \sigma_j^6}{2}\right)^{1/6}$$

$$\varepsilon_{ij} = 2\sqrt{\varepsilon_i \varepsilon_j}\,\frac{\sigma_i^3 \sigma_j^3}{\sigma_i^6 + \sigma_j^6}$$

We used forcefield parameters from the previous work[7] for the Nafion™ polymer, whereas parameters from the PCFF[8-10] forcefield were used for water (TIP3P) and NMP.

We first created solvent boxes containing water separately using 36412 and 6615 molecules of water and NMP, respectively. These solvent boxes were then energy minimized. To these geometry-optimized structures, Nafion™ chains were added. Before starting the MD runs, we performed geometry optimization of Nafion™ and solvent-containing simulation boxes. Then, the MD simulations were conducted with a time step $\Delta t = 1\, fs$ and using the Velocity-Verlet algorithm for integrating the equations of motion. The temperature of the system was maintained by a Nose-Hoover thermostat. To remove the effect of initial conditions and accelerate the evolution of the system towards equilibrium, we ran all our simulations for the first ns at a high temperature ($T = 1000\, K$) using canonical ensemble (NVT). Then, we annealed the system to T=300 K at the rate of 350 K/ns. Afterward, the temperature of the system was maintained at 300 K using an NVT ensemble for 2 ns. However, for the true sampling of the system, we applied the Isothermal–isobaric ensemble ($NVT\ with\ T = 300\, K, P = 1\, atm$) for 450 ns to reach the equilibrium state. In our MD simulations, we analyzed fluctuations in energy and structural parameters to confirm the achievement of the equilibrium state (**Figure S9**). We have specifically paid attention to variations in total energy from its mean value and the stability of sulfur-sulfur RDF plots over time (**Figure S10**). The energy fluctuation is described as follows:

$$\frac{\Delta \mathrm{E}}{\mathrm{E}} = \frac{\mathrm{E(t)} - |E_{mean}|}{|E_{mean}|}$$

Herein, for both water and NMP cases, the fluctuation in energy is very small $\left(\frac{\Delta \mathrm{E}}{\mathrm{E}} < 1\%\right)$. Also, structural properties such as sulfur-sulfur RDF converged within 150 ns for the NMP case. We confirmed that the systems reached an equilibrium state by ensuring that the fluctuations in energy are minimal and structural properties such as S-S RDFs and inter-ionic cluster distances of the system remain constant, **Figure S9,10**.

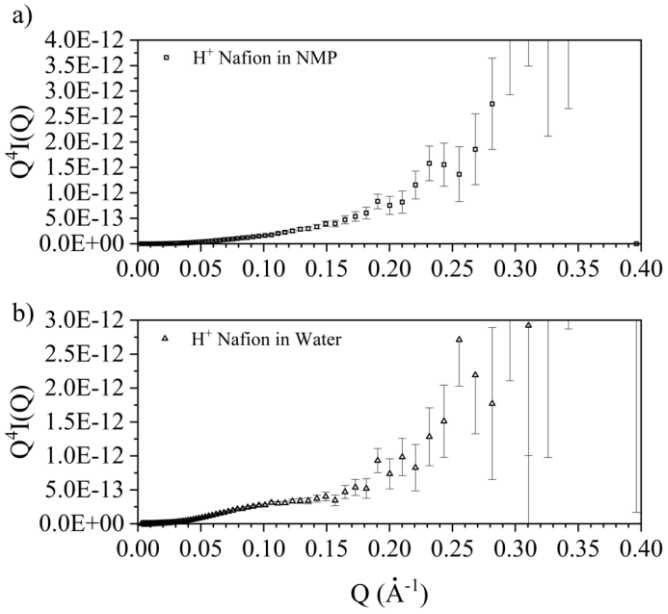


**Figure S2:** Porod plots of the SANS data corresponding to dispersions of a) $H^+$ Nafion in NMP, b) $H^+$ Nafion in Water.

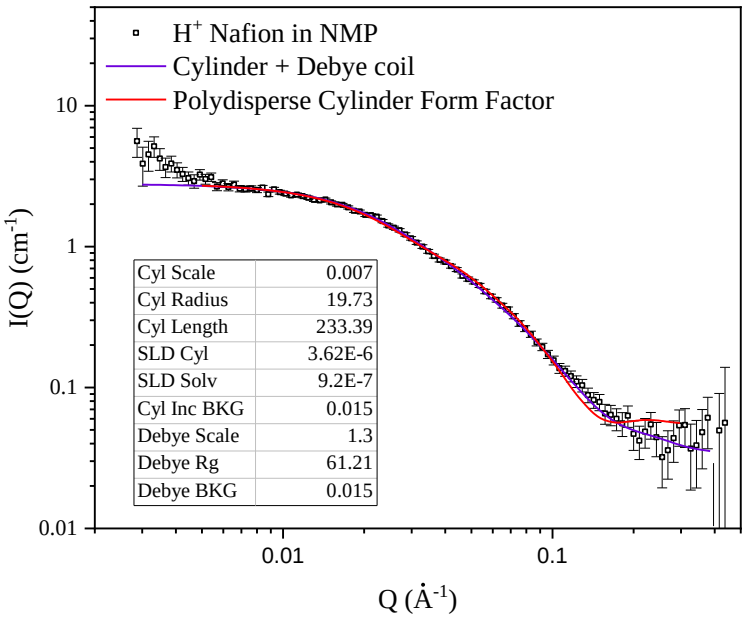


**Figure S3:** $H^+$ Nafion NMP dispersion, prepared by dilution, fit with a linear combination of a random coil and cylindrical form factor model.

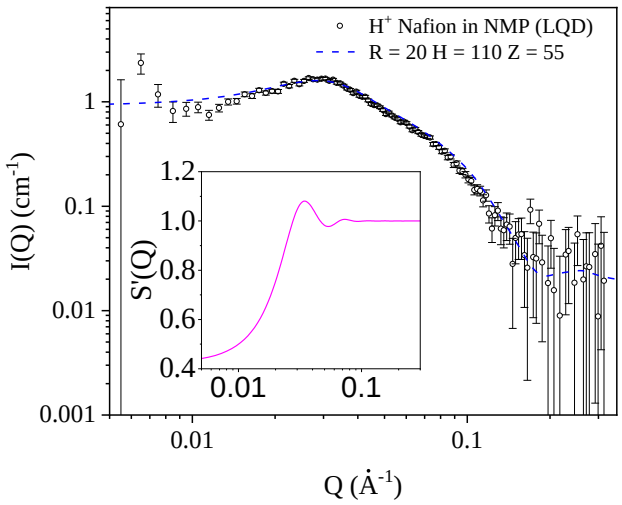


**Figure S4:** H+ Nafion™ in NMP from LQD fit with a structure factor model corresponding to a charged cylinder with 20 Å radius, 110 Å height, and a total charge of 55 $e^-$.

To generate the RMSA-based structure factor, the number of charged groups in the particle can be calculated. The number of charged species for a given volume element of Nafion™ was calculated for a single chain, as well as a volume element of multiple chains. The lower limit was calculated from the SANS profile of $Na^+$ Nafion™ in NMP previously reported.[6] A degree of polymerization was estimated from the intercept of the Debye fit to be 150. Knowing the mol% of charged monomers in Nafion™ 212 to be approximately 15 mol%, there are an estimated 22 charges per Nafion™ chain. An upper limit on the charge is estimated using the volume of the particle determined from a cylindrical form factor that fits the SANS profiles. Knowing the equivalent weight of Nafion™ 212 (1100), and the mass density of the Nafion™ particle from the SLD, a total of 152 charged groups for a 20 Å radius, 110 Å height cylinder are estimated. Based on the calculated limits of charged groups, it is estimated that Nafion™ particles in NMP will be composed of 1 – 7 individual Nafion chains. **Figure 4** shows the resulting model from calculating a structure factor for a particle with 55 charged groups in a 10 mM solution combined with a cylindrical form factor with R = 20 Å, H = 110 Å, and approximately 5 vol% NMP in the particle. From the weight percentage of Nafion™ in the original solution, the estimated concentration of acid is 20 mM, with a small degree of error expected.

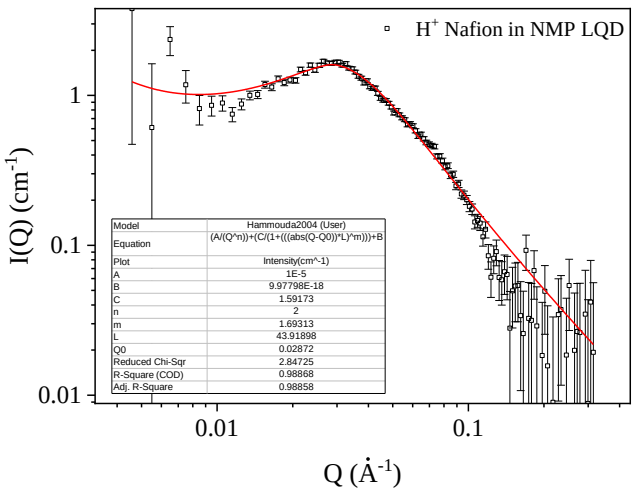


**Figure S5:** $H^+$ Nafion™ in NMP prepared by direct dispersion fit with Hammouda's swollen cluster equation[17].

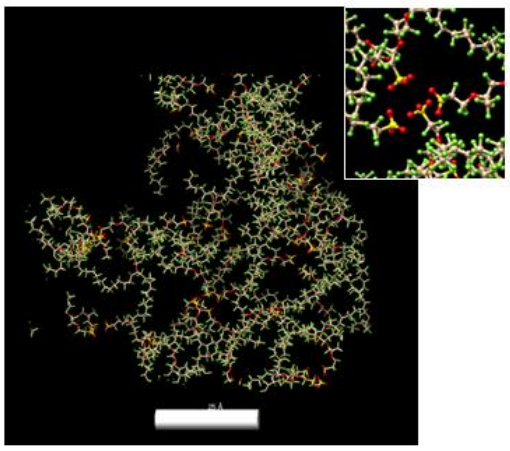

**Figure S6:** MD snapshot of 29 wt% Nafion™ dispersed in NMP. Scale bar shows 25 Å.

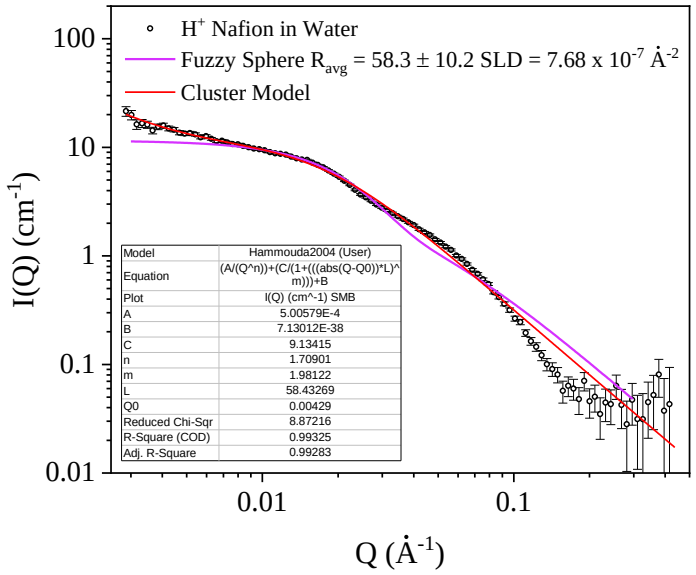


**Figure S7:** $H^+$ Nafion™ Dispersed in water fit with the cluster model.

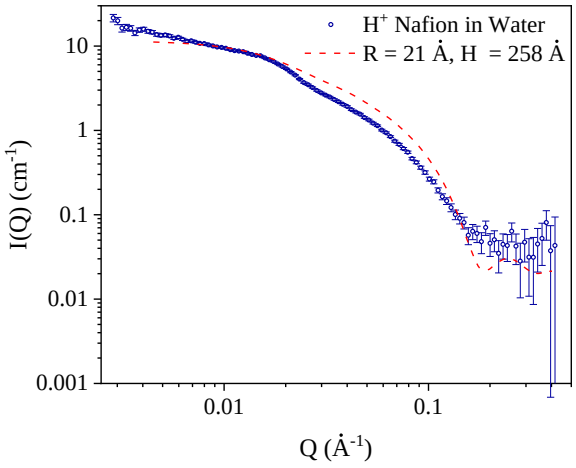


**Figure S8:** SANS profile of $H^+$ Nafion$^{TM}$ in water with the scattering of a theoretical particle whose dimensions match those determined by Guinier analysis.

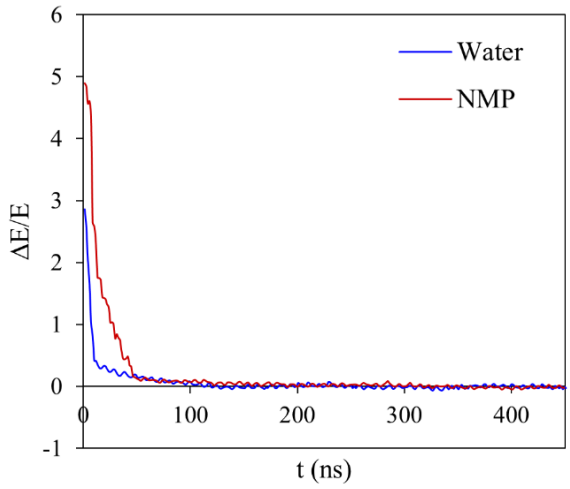


**Figure S9:** Energy fluctuation of the system during the run time

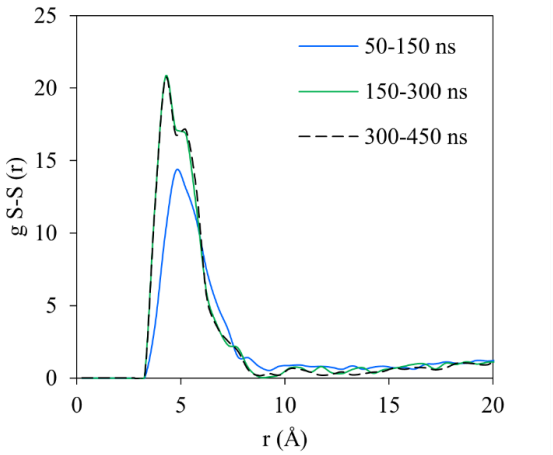


**Figure S10:** Radial Distribution Function of sulfur-sulfur atom in NMP during the run time

## References


1. Greene, D. G., Ferraro, D. V., Lenhoff, A. M. & Wagmer, N. J. A critical examination of the decoupling approximation for small-angle scattering from hard ellipsoids of revolution. *J. Appl. Crystallog.* **49**, 1734-1739.
2. Kim, D. S., Guiver, M. D., Welch, C. F., Hjelm, R. P. & Kim, Y. S. in *Comprehensive Polymer Science* Vol. 10 (eds K. Matyjaszewski & M. Möller) (Ch. 10.36, pp 691-720, Series Eds., Matyjaszewski, K.; Möller, M. Vol Eds., McGrath, J. E.; Hoefer, R.; Hickner M.A., Elsevier, New York, 2012).
3. Lei, C., Yang, F., Macauley, N., Spinetta, M., Purdy, G., Jankovic, J., Cullen, D. A., More, K. L., Kim, Y. S., Xu, H. Impact of catalyst ink dispersing solvent on PEM fuel cell performance and durability. *J. Electrochem. Soc.* **168**, 044517 (2021).
4. Kim, Y. S., Welch, C. F., Hjelm, R. P., Mack, N. H., Labouiau, A. & Orler, E. B. Origin of Toughness in dispersion-cast Nafion membranes. *Macromolecules* **48**, 2161-2172 (2015).
5. Kim, Y. S., Welch, C. F., Mack, N. H., Hjelm, R. P., Orler, E. B., Hawley, M. E., Lee, K. S., Yim, S. D. & Johnson, C. Highly durable fuel cell electrodes based on ionomers dispersed in glycerol. *Phys. Chem. Chem. Phys.* **16**, 5927-5932 (2014).
6. Welch, C., Labouriau, A., Hjelm, R., Orler, B., Johnston, C. & Kim, Y. S. Nafion in dilute solvent systems: Dispersion or solution? *ACS Macro Lett.* **1**, 1403-1407 (2012).
7. Kline, S. R. Reduction and analysis of SANS and USANS data using IGOR Pro. *J. Appl. Crystallog.* **39**, 895-900 (2006).
8. Kotlarchyk, M. & Chen, S.-H. Analysis of small angle neutron scattering spectra from polydisperse interacting colloids. *J. Chem. Phys.* **79**, 2461-2469 (1983).
9. Ashcroft, N. W. & Lekner, J. Structure and resistivity of liquid metals. *Phys. Rev.* **145**, 83-90 (1966).
10. Kinning, D. J. & Thomas, E. L. Hard-sphere interactions between spherical domains in diblock copolymers. *Macromolecules* **17**, 1712-1718 (1984).
11. Hansen, J.-P. & Hayter, J. B. A rescaled MSA structure factor for dilute charged colloidal dispersions. *Mol. Phys.* **46**, 651-656 (1982).
12. Hayter, J. B. & Penfold, J. An analytic structure factor for macroion solutions. *Molecular Physics* **42**, 109-118 (1981).
13. Heinen, M., Holmqvist, P., Banchio, A. J. & Nägele, G. Pair structure of the hard-sphere Yukawa fluid: An improved analytic method versus simulations, Rogers-Young scheme, and experiment. *J. Chem. Phys.* **134**, 044532 (2011).
14. Heinen, M., Holmqvist, P., Banchio, A. J. & Nägele, G. Erratum: Pair structure of the hard-sphere Yukawa fluid: An improved analytic method versus simulations, Rogers-Young scheme, and experiment *J. Chem. Phys.* **134**, 129901 (2011).
15. Snook, I. K. & Hayter, J. B. Static structure of strongly interacting colloidal particles. *Langmuir* **8**, 2880-2884 (1992).
16. Loppinet, B., Gebel, G. & Williams, C. E. Small-angle scattering study of perfluorosulfonated ionomer solutions. *J. Phys. Chem. B* **101**, 1884-1892 (1997).
17. Hammouda, B., Ho, D. L. & Kline, S. Insight into clustering in poly(ethylene oxide) solutions. *Macromolecules* **37**, 6932-6937 (2004).
18. Guinier, A. & Fournet, G. *Small-angle scattering of X-rays*. (John Wiley and Sons, 1955).
19. Stieger, M., Pedersen, J. S., Lindner, P. & Richtering, W. Are thermoresponsive microgels model systems for concentrated colloidal suspensions? A rheology and small-angle neutron scattering study. *Langmuir* **20**, 7283-7292 (2004).

1 Greene, D. G., Ferraro, D. V., Lenhoff, A. M. & Wagner, N. J. A critical examination of the decoupling approximation for small-angle scattering from hard ellipsoids of revolution. *Journal of Applied Crystallography* **49**, 1734-1739, doi:10.1107/S1600576716012929 (2016).
2 Sokolova, A. *et al.* Performance and characteristics of the BILBY time-of-flight small-angle neutron scattering instrument. *Journal of Applied Crystallography* **52**, 1-12, doi:10.1107/S1600576718018009 (2019).
3 Hjelm, R. P. The Resolution of TOF Low-Q Diffractometers: Instrumental, Data Acquisition and Reduction Factors. *Journal of Applied Crystallography* **21**, 618-628 (1988).
4 Seeger, P. A. & Hjelm, R. P. Small-Angle Neutron Scattering at Pulsed Spallation Sources. *Journal of Applied Crystallography* **24**, 467-478 (1991).
5 Arnold, O. *et al.* Mantid—Data analysisandvisualizationpackageforneutronscattering and μ SR experiments. *Nuclear Instruments and Methods in Physics Research A* **764**, 156-166, doi:10.1016/j.nima.2014.07.029 (2014).
6 Plimpton, S. FAST PARALLEL ALGORITHMS FOR SHORT-RANGE MOLECULAR-DYNAMICS. *JOURNAL OF COMPUTATIONAL PHYSICS* **117**, 1-19, doi:10.1006/jcph.1995.1039 (1995).
7 Jinnouchi, R., Kudo, K., Kitano, N. & Morimoto, Y. Molecular dynamics simulations on O-2 permeation through nafion ionomer on platinum surface (vol 188, pg 767, 2016). *ELECTROCHIMICA ACTA* **287**, 160-160, doi:10.1016/j.electacta.2018.07.144 (2018).
8 Maple, J. R. *et al.* DERIVATION OF CLASS-II FORCE-FIELDS .1. METHODOLOGY AND QUANTUM FORCE-FIELD FOR THE ALKYL FUNCTIONAL-GROUP AND ALKANE MOLECULES. *JOURNAL OF COMPUTATIONAL CHEMISTRY* **15**, 162-182, doi:10.1002/jcc.540150207 (1994).
9 Sun, H. FORCE-FIELD FOR COMPUTATION OF CONFORMATIONAL ENERGIES, STRUCTURES, AND VIBRATIONAL FREQUENCIES OF AROMATIC POLYESTERS. *JOURNAL OF COMPUTATIONAL CHEMISTRY* **15**, 752-768, doi:10.1002/jcc.540150708 (1994).
10 Sun, H., Mumby, S. J., Maple, J. R. & Hagler, A. T. AN AB-INITIO CFF93 ALL-ATOM FORCE-FIELD FOR POLYCARBONATES. *JOURNAL OF THE AMERICAN CHEMICAL SOCIETY* **116**, 2978-2987, doi:10.1021/ja00086a030 (1994).